Special Issue

Optical Coherence Tomography Angiography Analysis of Perfused Peripapillary Capillaries in Primary Open-Angle Glaucoma and Normal-Tension Glaucoma

Nicole K. Scripsema,[1] Patricia M. Garcia,[1] Richard D. Bavier,[1,2] Toco Y. P. Chui,[1] Brian D. Krawitz,[1] Shelley Mo,[1] Steven A. Agemy,[1,3] Luna Xu,[1] Yijie B. Lin,[1] Joseph F. Panarelli,[1] Paul A. Sidoti,[1] James C. Tsai,[1] and Richard B. Rosen[1]

[1]Department of Ophthalmology, The New York Eye and Ear Infirmary of Mount Sinai and Icahn School of Medicine at Mount Sinai, New York, New York, United States
[2]Rutgers New Jersey Medical School, Newark, New Jersey, United States
[3]Department of Ophthalmology, SUNY Downstate Medical Center and SUNY Downstate College of Medicine, Brooklyn, New York, United States

Correspondence: Richard B. Rosen, 310 East 14th Street, 5th Floor South Building, New York, NY 10003, USA; RRosen@nyee.edu.

Submitted: December 14, 2015
Accepted: August 19, 2016

Citation: Scripsema NK, Garcia PM, Bavier RD, et al. Optical coherence tomography angiography analysis of perfused peripapillary capillaries in primary open-angle glaucoma and normal-tension glaucoma. *Invest Ophthalmol Vis Sci*. 2016;57:OCT611–OCT620. DOI: 10.1167/iovs.15-18945

Purpose. To compare perfused peripapillary capillary density in primary open-angle glaucoma (POAG), normal-tension glaucoma (NTG), and normal patients using optical coherence tomography angiography (OCT-A).

Methods. A retrospective review of POAG, NTG, and normal patients imaged with OCT-A was performed. En face OCT angiograms identifying peripapillary vessels were obtained using a spectral-domain OCT system (Avanti RTVue-XR). A custom image analysis approach identified perfused peripapillary capillaries, quantified perfused capillary density (PCD), and generated color-coded PCD maps for 3.5- and 4.5-mm-diameter scans. We compared PCD values, PCD maps, standard automated perimetry (Humphrey visual field [HVF]) parameters, and OCT retinal nerve fiber layer (RNFL) thickness analyses across all groups.

Results. Forty POAG, 26 NTG, and 26 normal patients were included. Annular PCD in POAG (34.24 ± 6.76%) and NTG (37.75 ± 3.52%) patients was significantly decreased compared to normal patients (42.99 ± 1.81%) in 4.5-mm scans ($P < 0.01$ and $P < 0.01$, respectively). Similar trends and statistical significances were seen in 3.5-mm scans. Linear regression analysis resulted in moderate correlations between annular PCD values and other glaucomatous parameters. Pearson coefficients comparing annular PCD from 4.5-mm scans in POAG and NTG groups to HVF mean deviation, HVF pattern standard deviation, and average RNFL thickness all showed statistical significance ($P < 0.05$). Color maps showed that POAG and NTG patients had a reduction of perfused capillaries that progressed in size when comparing early, moderate, and severe glaucoma groups.

Conclusions. Optical coherence tomography angiography can uniquely identify changes in peripapillary PCD in glaucoma patients. Optical coherence tomography angiography may offer insights into the pathophysiology of glaucomatous damage and risk factors for disease progression.

Keywords: optical coherence tomography, glaucoma posterior segment, angiography, low-tension glaucoma, optic nerve head

Glaucoma is one of the leading causes of blindness worldwide, currently afflicting more than 60 million people and predicted to affect 79.6 million people by 2020.[1–3] Given the insidious course and irreversible damage caused by glaucoma, early diagnosis, prompt treatment, and close monitoring are critical in disease management. Even when optimal intraocular pressure lowering is consistently achieved, a subset of patients continue to progress. The pathophysiological theories correlating high intraocular pressure (IOP) with mechanical optic nerve damage cannot always account for this progression. Studies suggest that vascular dysfunction causing optic nerve hypoperfusion may contribute to glaucoma progression in patients with both high and normal IOPs.[4–9] Alterations in systemic blood pressure or vasospasm may result in low ocular perfusion pressure, defined as the difference between systemic blood pressure and IOP. Several studies including the Baltimore Eye Survey and the Barbados Eye Study have identified both high IOP and low ocular perfusion pressure as risk factors for glaucomatous nerve damage.[10–14] The role of systemic hypertension in glaucomatous damage is less well established, with varied reports in the literature.[6,10,11,15–18] Hypotension, particularly nocturnal hypotension, has shown increasing evidence as a strong risk factor for disease progression.[19–26] Despite this evidence, our understanding of the role of optic nerve perfusion in the pathophysiology of glaucoma is limited.

Standard automated perimetry remains the gold standard for visual field testing and glaucoma assessment. While perimetry provides information essential for the proper management of the disease and interobserver reproducibility among glaucoma

experts is high, visual fields often have substantial intertest variability.[27,28] Consequently, objective tests that analyze the optic disc structure are increasingly used in the assessment of glaucoma.[29–32] Optical coherence tomography (OCT) analysis of peripapillary retinal nerve fiber layer (RNFL) thickness is one of several modalities currently used as an objective, quantifiable measure for detecting glaucoma and assessing progression.[33–38]

Optical coherence tomography angiography (OCT-A) is a novel technique that employs en face reconstruction of OCT combined with motion contrast processing to reveal perfused retinal vasculature. Split-spectrum amplitude-decorrelation angiography (SSADA) algorithm detects the movement of red blood cells within retinal and choroidal vessels to generate angiographic images of perfused vessels in a fast, reliable, and noninvasive manner.[39] Currently, the SSADA algorithm can provide images of perfused capillaries in both the perifoveal and peripapillary regions. As the neuroretina has a high metabolic demand, insights into the status of the retinal microvasculature could be an excellent indicator of the presence or potential for disease. In a previous study, our group demonstrated the use of perifoveal OCT-A imaging in the staging of diabetic retinopathy.[40] Other groups have reported the utility of optic disc and peripapillary OCT-A imaging for several conditions, including glaucoma.[41–45] A study analyzing peripapillary glaucomatous changes with OCT-A reported a decrease in perfused peripapillary vasculature in glaucoma patients compared to normal subjects.[42]

The purpose of the present study was to determine if OCT-A is capable of differentiating normal eyes versus glaucomatous eyes, and if our custom image analysis approach that provides qualitative and quantitative analysis of the perfused peripapillary capillaries, defined as the network of capillaries from the inner limiting membrane (ILM) to the posterior boundary of the RNFL, can detect variations between primary open-angle glaucoma (POAG), normal-tension glaucoma (NTG), and normal patients.

Methods

Study Population

This retrospective review was conducted at the Bendheim-Lowenstein Retina Center of the New York Eye and Ear Infirmary of Mount Sinai. The research study adhered to the tenets of the Declaration of Helsinki and was approved by the Institutional Review Board of the New York Eye and Ear Infirmary of Mount Sinai.

Primary open-angle glaucoma, NTG, and normal patients imaged with OCT-A from April 2015 to August 2015 were included. Glaucomatous optic neuropathy was defined based on clinical exam findings including focal or diffuse neuroretinal rim thinning, focal or diffuse RNFL loss, or an intereye vertical cup-to-disc ratio (CDR) asymmetry of >0.2 not explained by differences in disc size. An open angle on gonioscopy was also required. All patients required documentation by a glaucoma specialist confirming these clinical findings on a minimum of two visits. Most patients included have been followed in our clinic for years. Inclusion criteria for POAG patients required a history of elevated IOP (>24 mm Hg) either with or without treatment. Inclusion criteria for NTG patients were a history of untreated peak IOP of 21 mm Hg or less. All glaucoma patients meeting these criteria were also required to have at least two reproducible visual field tests with glaucomatous defects. A minimal visual field defect consisted of a cluster of three adjacent points depressed by at least 5 dB from normal age values, with one of these points depressed by at least 10 dB from normal age values. At least three points of such a cluster were required to be on one side of the horizontal meridian, with other points elsewhere at least 10 dB higher than the densest point in the scotoma. Peak IOP, IOP on the day of imaging, central corneal thickness (CCT), age, current glaucoma treatment, and surgical history were also recorded for each patient. Patients with prior cataract extraction or glaucoma surgery were not excluded. Exclusion criteria included diabetes mellitus, hypertension, or other ocular conditions with the exception of cataract or prior cataract extraction. All patients had undergone a complete ophthalmic examination, including best-corrected visual acuity, slit-lamp biomicroscopy, gonioscopy, and Goldmann applanation tonometry on the day of OCT-A. A dilated fundus exam was performed on all patients within 6 months of imaging. Only patients with Humphrey visual field (HVF), OCT RNFL thickness analysis, and disc photos performed within 1 month of imaging were included.

Visual Field Testing

Patients were included only if they had a reliable visual field performed within 1 month of imaging. Reliable performance on visual field testing was defined as fixation errors < 20%, false positives < 15%, and false negatives < 33%. Visual fields were performed with the Humphrey Field Analyzer II (Carl Zeiss Meditec, Inc., Dublin, CA) using a 24-2 threshold test with size III white stimulus and a standard SITA (Swedish interactive thresholding algorithm). Patients with visual field abnormalities had at least one confirmatory examination. Mean deviation (MD) and pattern standard deviation (PSD) were used to compare to OCT-A data. In addition, patients were categorized into early, moderate, or severe glaucoma subgroups based on the Hodapp-Anderson-Parrish (HAP) Visual Field Severity Score.[46]

OCT Circumpapillary Retinal Nerve Fiber Layer Analysis

Optical coherence tomography RNFL thickness analysis (Cirrus HDT OCT 500; Carl Zeiss Meditech, Inc.) was performed prior to OCT-A. Average RNFL thickness and RNFL quadrant analysis were used for comparison with OCT-A data. Analyses with signal strengths of less than 7/10 were excluded.

OCT-A Image Acquisition

Optical coherence tomography angiography images were obtained with a commercial spectral-domain OCT system (Avanti RTVue-XR; Optovue, Fremont, CA, USA) as previously described.[40] Each patient underwent a single imaging session consisting of both 3.5 × 3.5-mm-diameter peripapillary scans (3.5-mm) and 4.5 × 4.5-mm-diameter peripapillary scans (4.5-mm scan). Patients whose images had inadequate signal strength were excluded. Assessment of adequate signal strength was achieved by analysis of the resulting OCT-A image. When the OCT-A image is poor due to significant motion artifact or low signal strength, the image contains lines or gaps indicating insufficient information for complete angiographic reconstruction. Images with these OCT-A artifacts were excluded.

A SSADA algorithm was used to identify perfused vessels, including larger retinal vessels and the surrounding capillary network, for each scan. The specifics of similar algorithms have been previously published.[41,43,47–50] To summarize briefly, the algorithm distinguishes the movement of red blood cells within the lumen of retinal and choroidal vessels between cross-sectional scans. The decorrelation algorithm identifies per-

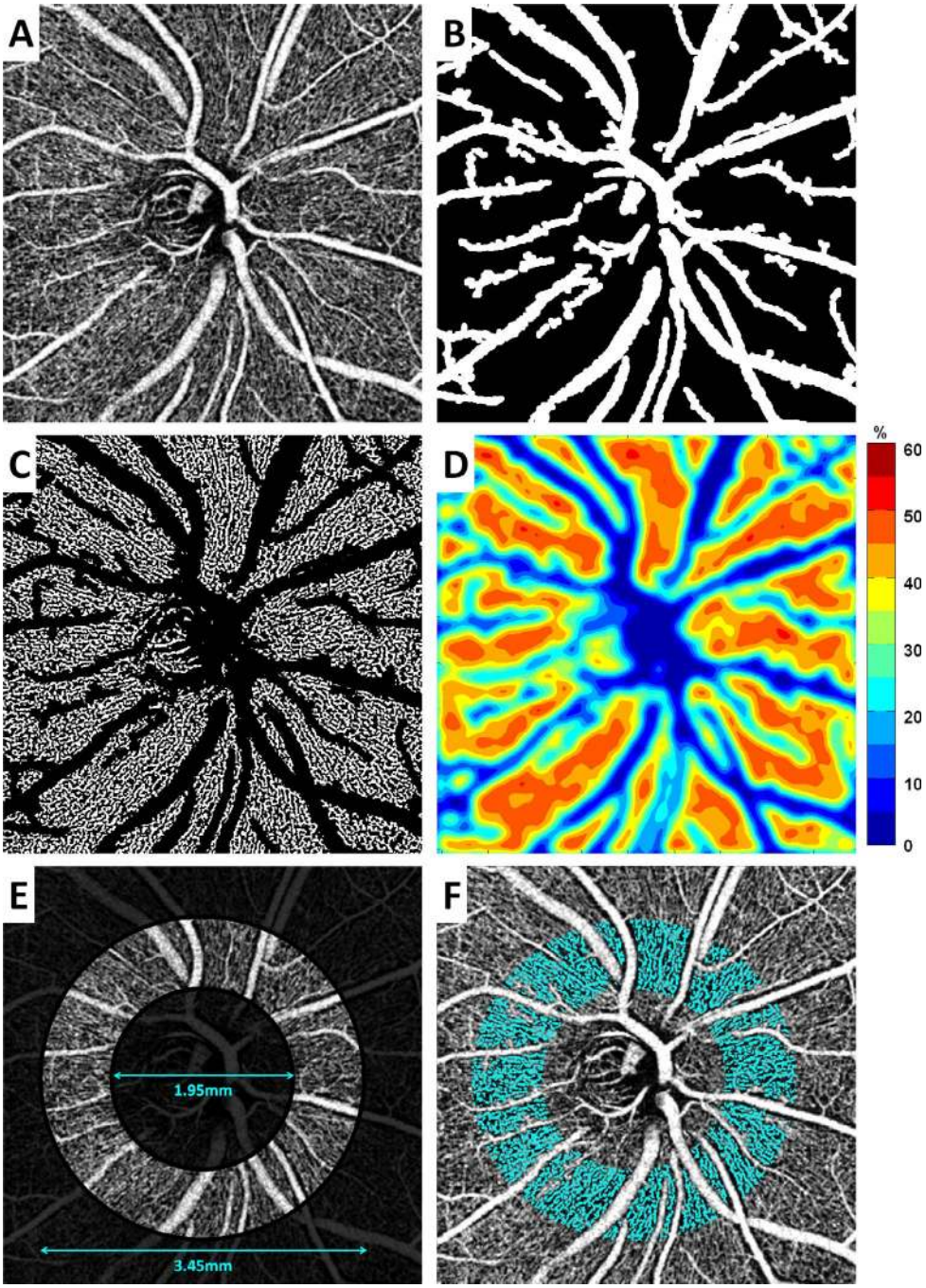

FIGURE 1. OCT-A image processing steps. (**A**) Contrast-stretched grayscale 4.5-mm OCT-A image of a healthy control. (**B**) Major blood vessel mask created using global thresholding. (**C**) Binary image after local adaptive thresholding with major blood vessels removed. (**D**) Color-coded perfused capillary density map. (**E**) Annular ROI centered at the optic nerve head. (**F**) Perfused capillary area within the annular ROI (in *cyan*) superimposed with (**A**).

fused retinal vessel from surrounding static tissue based upon signal amplitude variation differences in nonstatic tissue compared to static tissue. It cannot quantitate flow differences below a certain threshold of motion, meaning that vessels with slow or no flow are not visualized with this technique.

Subject movements during image acquisition also generate decorrelation, which must be compensated for in order to yield acceptable vascular maps. The Optovue software (Motion Correction Technology MCT) compensates for motion artifacts by combining matching horizontal-priority and vertical-priority scan volumes using an orthogonal registration algorithm to

TABLE 1. Demographic Data of Study Groups

Study Group	*N*, Subjects	% Male	Age	*P* Value*
POAG	40	55	66.30 ± 11.49	0.34
NTG	26	34	67.92 ± 9.35	
Normal	26	38	63.72 ± 9.07	

* No statistically significant difference was observed between study groups with respect to age (1-way ANOVA).

Table 2. Glaucoma Severity in POAG and NTG Groups

Glaucoma Severity	POAG Patients, No. (%)	NTG Patients, No. (%)
Early	22 (55)	13 (50)
Moderate	6 (15)	7 (27)
Severe	12 (30)	6 (23)
Total	40	26

Based on Hodapp-Anderson-Parrish Visual Field Severity Score.

remove bulk motion and produce a merged OCT image volume with essentially no residual motion artifacts.[51] It also calculates the mean decorrelation and subtracts this value from each frame, setting the decorrelation value for bulk tissue to approximately zero, allowing for the creation of en face OCT angiograms.

In this study we analyzed the perfused peripapillary vasculature, which includes the larger blood vessels as well as peripapillary capillaries located between ILM and the posterior boundary of RNFL. The Optovue built-in software automatically segments these two boundaries on the OCT scans and performs z-projection of the maximum decorrelation value to generate an en face OCT-A image (Fig. 1A). The OCT-A images of all patients were reviewed to ensure proper segmentation of OCT scans. Although both eyes were imaged, only a single eye from each patient was selected at random and included for data analysis to avoid potential interocular correlation between eyes.

OCT-A Image Analysis

All OCT-A images were analyzed using a custom-developed MATLAB program (The Mathworks, Inc., Natick, MA, USA). First, each grayscale OCT-A image (304 × 304 pixels) was resized by a factor of six (1824 × 1824 pixels). Each resized image was contrast stretched by using the lowest and highest 1% pixel intensity values of the image as the lower and upper limits, respectively. Then, global thresholding was performed to convert the contrast-stretched grayscale OCT-A image into a binary image by replacing all pixel intensity greater than the level value of 0.55 on the grayscale OCT-A image with the value 1 (white) and the remaining pixels with the value 0 (black). This binary image was used as a mask (Fig. 1B) for the removal of the pixels associated with the major blood vessels on the OCT-A image. After the removal of major blood vessels on the contrast-stretched grayscale OCT-A, a second image thresholding was performed using a local adaptive thresholding algorithm with a sampling window size of 15 × 15 pixels. This final binary image contains only the perfused peripapillary capillaries (Fig. 1C).

OCT-A Qualitative Analysis: Color-Coded Perfused Capillary Density Maps

A color-coded perfused capillary density (PCD) map was generated by computing capillary area density within each 16-× 16-pixel sampling window with 8-pixel overlaps over the final binary image (Fig. 1C). This color-coded density map allowed for quick interpretation and better visualization of regional peripapillary capillary density variations across the entire OCT-A image (Fig. 1D). In the color maps, bright red indicates a high density of perfused capillaries, dark blue indicates area of low or no perfused capillaries, and intermediate densities are represented on a spectrum of yellow to green. Larger retinal vessels excluded from the analysis also appear blue on the color maps.

OCT-A Quantitative Analysis: Annular Perfused Capillary Density (%)

To ensure that the same region of interest (ROI) was included in all OCT-A images, PCD within a fixed annular ROI centered at the optic nerve head was extracted for quantitative analysis. In brief, two concentric circles with 1.95-mm (inner) and 3.45-mm (outer) diameters were placed manually by an experienced examiner, producing an annular ROI with a width of 0.75 mm (Figs. 1E, 1F). This 3.45-mm outer circle diameter represented the standard circumpapillary scan dimension for RNFL thickness measurement that is currently employed in the majority of commercially available OCT systems. Annular PCD was calculated by the number of pixels associated with perfused capillaries over the number of pixels in the annular ROI after the removal of major blood vessels. These analyses were performed for all controls and glaucoma patients using both 3.5- and 4.5-mm OCT-A images.

Global Perfused Capillary Density (%)

Global PCD was calculated by generating a percentage of the number of pixels associated with perfused capillaries over the number of pixels in the entire image after removal of the inner 1.95-mm circular area and the major blood vessels. These analyses were also performed for all controls and patients with glaucoma using the 3.5- and 4.5-mm OCT-A images.

Repeatability and Reproducibility

The repeatability and reproducibility of the Optovue Avanti were previously published and are consistent with the literature.[40,41,43–45,52] Optical coherence tomography angiography has excellent repeatability and reproducibility indices.

Statistical Analysis

Linear regression analysis was used to investigate the relationship between PCD and other variables, including average OCT RNFL thickness, HVF MD, HVF PSD, age, and IOP. Comparisons were made with both annular and global PCD for 3.5- and 4.5-mm scans. The means, standard deviations, and Pearson's correlation coefficient (r) were calculated. In both 3.5- and 4.5-mm scans, annular and global PCD were compared among the POAG, NTG, and normal

Table 3. Glaucoma Parameters for POAG, NTG, and Normal Patients

Study Group	HVF MD, Mean ± SD	*P* Value	Average RNFL, µm, Mean ± SD	*P* Value	CDR, Mean ± SD	*P* Value	Tmax, mm Hg, Mean ± SD	*P* Value	CCT, µm, Mean ± SD	*P* Value
POAG	−8.84 ± 9.58	0.82	69.10 ± 14.06	0.25	0.76 ± 0.17	0.91	26.43 ± 8.94	<0.01*	538.58 ± 37.91	0.35
NTG	−8.33 ± 7.25		73.25 ± 15.25		0.76 ± 0.09		18.04 ± 1.82		530.08 ± 33.26	
Normal	−1.43 ± 1.27		96.04 ± 9.72		0.32 ± 0.15		20.15 ± 5.08		543.54 ± 44.44	

Comparisons were made between POAG and NTG patients to demonstrate a similar severity of glaucoma across the groups.
* $P < 0.05$ was considered statistically significant (unpaired t-test).

Table 4. Annular Perfused Capillary Density (PCD) Values in POAG, NTG, and Normal Patients

Study Group	Annular PCD, 3.5-mm Scan, Mean ± SD	*P* Value*	*P* Value†	Annular PCD, 4.5-mm Scan, Mean ± SD	*P* Value*	*P* Value†
POAG	33.40 ± 6.53%	<0.01‡	<0.05‡	34.24 ± 6.76%	<0.01‡	<0.05‡
NTG	37.20 ± 3.51%	<0.01‡		37.75 ± 3.52%	<0.01‡	
Normal	42.45 ± 1.56%			42.99 ± 1.81%		

* *P* value of glaucoma group versus normal.
† *P* value of POAG versus NTG.
‡ *P* value < 0.05 was considered statistically significant (1-way ANOVA, Tukey's HSD test).

groups by 1-way analysis of variance (ANOVA). Tukey's honest significant difference (HSD) test was applied for post hoc pairwise comparisons between groups. Unpaired *t*-tests were performed for the comparisons of the glaucoma parameters between POAG and NTG groups. Mann-Whitney *U* test was used to compare PCD values between early, moderate, and severe glaucoma subgroups. All analysis was performed with statistical software (SPSS, version 23.0; IBM, Corp., Armonk, NY, USA). Qualitative analysis was also performed to compare color-coded PCD maps to average RNFL thickness.

Results

The charts of 137 patients imaged with OCT-A were reviewed. After excluding patients based on the criteria listed above, a total of 92 patients were included. A total of 22 POAG, 16 NTG, and 7 normal patients were excluded. A majority of patients were excluded due to unreliable visual fields (71%) or poor image quality secondary to poor fixation or the presence of a visually significant cataract (29%).

A single eye from 40 POAG, 26 NTG, and 26 normal patients was included. Mean age was 66.05 ± 10.29 years overall, and using ANOVA was found to be similar among all groups (1-way ANOVA, $P = 0.34$, Table 1). Males represented 46% of all patients, also similar across all groups (1-way ANOVA, $P = 0.66$, Table 1). A total of 62% of patients were Hispanic, 20% African American, 14% Caucasian, and 10% Asian. This distribution was similar across all groups (1-way ANOVA, $P = 0.45$). There was an equal distribution of early, moderate, and severe glaucoma patients in the POAG and NTG groups based on the HAP Visual Field Severity Scale (Table 2).[46] The distribution in the POAG group was 55% early, 15% moderate, and 30% severe. The NTG group was similarly distributed, with 50% early, 27% moderate, and 23% severe.

There was no significant difference between mean HVF MD, average RNFL thickness, CDR, and CCT in the glaucoma groups (Table 3). Mean peak IOP (Tmax), determined by chart review, was significantly different between POAG (26.43 ± 8.94 mm Hg) and NTG (18.03 ± 1.82 mm Hg) groups (unpaired *t*-test, $P < 0.01$). Mean IOP on the day of imaging (Ta) was also statistically significantly different between POAG (14.85 ± 3.40 mm Hg), NTG (12.69 ± 2.57 mm Hg), and normal groups (15.90 ± 2.98 mm Hg, 1-way ANOVA, $P = 0.001$). Treatment also varied between the groups. Primary open-angle glaucoma patients were treated with an average of 2.76 ± 1.08 eye drops, while NTG patients were treated with an average of 1.88 ± 1.14 eye drops (unpaired *t*-test, $P < 0.01$). In the POAG group 15% used a prostaglandin analogue alone, 17% in combination with dorzolamide-timolol, and 68% both these medications in addition to brimonidine. In the NTG group 54% used a prostaglandin analogue alone, 15% in combination with dorzolamide-timolol, and 31% both medications in addition to brimonidine. Nine (22%) POAG patients and four (15%) NTG patients underwent prior cataract extraction. Four (10%) POAG patients and two (8%) NTG patients underwent previous glaucoma surgery. Trabeculectomy (83%) was more common than tube shunt surgery (17%).

The comparison of annular PCD in POAG, NTG, and normal patients is displayed in Table 4. Annular PCD represents the percent of pixels associated with perfused capillaries over the total number of pixels in the annular ROI after removal of the major blood vessels. Annular PCD for the 3.5-mm scans was 33.40 ± 6.53% for POAG, 37.20 ± 3.51% for NTG, and 42.45 ± 1.56% for normal patients. Annular PCD for the 4.5-mm scans was 34.24 ± 6.76% for POAG, 37.75 ± 3.52% for NTG, and 42.99 ± 1.81% for normal patients. There were statistically significant differences between group means for both 3.5- and 4.5-mm scans (1-way ANOVA, $P < 0.01$). Post hoc pairwise comparisons between groups indicated that annular PCD for both 3.5- and 4.5-mm scans was significantly reduced in both POAG and NTG groups when compared to normal ($P < 0.01$). Annular PCD was also significantly reduced in the POAG group when compared to the NTG group ($P < 0.01$).

Using our custom software, a global PCD analysis of each image, after the removal of both the inner 1.95-mm circular area and the major blood vessels, was also performed (Table 5). We found similar trends and statistical significances in the global PCD values when compared to the annular PCD (Fig. 1E).

While the sample sizes in the early, moderate, and severe glaucoma groups were limited, both POAG and NTG patients demonstrated decreased annular PCD as glaucoma severity increased. The only statistically significant changes were between early and moderate glaucoma in both POAG (Mann-Whitney *U* test, $P = 0.01$) and NTG ($P = 0.04$) groups (Table 6) and between early and severe glaucoma in the POAG group (*P*

Table 5. Global Perfused Capillary Density (PCD) Values in POAG, NTG, and Normal Patients

Study Group	Global PCD, 3.5-mm Scan, Mean ± SD	*P* Value*	*P* Value†	Global PCD, 4.5-mm Scan, Mean ± SD	*P* Value*	*P* Value†
POAG	33.13 ± 6.23%	<0.01‡	<0.05‡	33.31 ± 6.49%	<0.01‡	<0.05‡
NTG	36.49 ± 3.18%	<0.01‡		36.48 ± 3.10%	<0.01‡	
Normal	41.32 ± 1.96%			41.88 ± 2.16%		

* *P* value of glaucoma group versus normal.
† *P* value of POAG versus NTG.
‡ *P* value < 0.05 was considered statistically significant (1-way ANOVA, Tukey's HSD test).

Table 6. Annular Perfused Capillary Density (PCD) by Glaucoma Stage

Glaucoma Severity	POAG Annular PCD, 4.5-mm Scan	NTG Annular PCD, 4.5-mm Scan
Early	38.01 ± 3.66%	39.16 ± 2.56%
Moderate	32.65 ± 3.63%*	36.42 ± 2.94%*
Severe	26.89 ± 6.52%*	36.25 ± 5.05%
Total	34.24 ± 6.76%	37.75 ± 3.52%

* Statistically significant difference compared to early glaucoma ($P < 0.05$, Mann-Whitney U test).

< 0.01). The comparison between early and severe glaucoma in NTG was not statistically significant ($P = 0.19$), likely as a result of a small sample size and higher standard deviation in comparison to the other groups.

There was a moderate linear relationship between average RNFL thickness and annular PCD for POAG and normal patients reaching statistical significance in both 3.5- and 4.5-mm scans (Fig. 1). Pearson correlation for the POAG group was $r = 0.74$ ($P < 0.01$) and $r = 0.69$ ($P < 0.01$), respectively. This correlation was weaker for NTG patients; however, it did still reach statistical significance ($r = 0.50$, $P = 0.01$ and $r = 0.45$, $P = 0.02$, respectively). Humphrey visual field MD and HVF PSD also showed moderate correlation with annular PCD values, again with the POAG group showing stronger correlation than the NTG group. Pearson correlation for HVF MD in the 4.5-mm scans was $r = 0.72$ ($P < 0.01$) for the POAG group and $r = 0.50$ ($P = 0.01$) for the NTG group. Pearson correlation for HVF PSD in the 4.5-mm scan was $r = 0.61$ ($P < 0.01$) in the POAG group and $r = 0.46$ ($P = 0.02$) in the NTG group. Similar correlations were demonstrated in the 3.5-mm scans. In both the POAG and NTG groups there was no significant correlation between annular PCD values and age ($r = 0.10$, $P = 0.47$ and $r = 0.32$, $P = 0.12$, respectively) or IOP ($r = 0.22$, $P = 0.18$ and $r = 0.10$, $P = 0.66$), respectively). We also analyzed the correlation between 3.5- and 4.5-mm annular PCD values, which showed a very strong correlation ($r = 0.94$, $P < 0.001$). Graphs correlating 4.5-mm annular PCD values with 3.5-mm annular PCD values, age, HVF MD, HVF PSD, RNFL, and IOP are shown in Figures 2A through 2D.

The linear correlation between annular PCD values, mean HVF MD, mean HVF PSD, and mean OCT RNFL thickness suggests that as glaucoma progresses, annular PCD decreases. Analysis of the color-coded PCD maps showed that when comparing color maps in early, moderate, and severe POAG and NTG patients as glaucoma advances, areas lacking perfused capillaries become larger as glaucoma progresses (Fig. 3).

Discussion

Previous studies demonstrate the use of OCT with a SSADA algorithm in the detection of microvascular changes in both the perifoveal and peripapillary regions in diseased eyes.[40,42–44,47,50,53–55] Split-spectrum amplitude-decorrelation angiography is a technique first described by Jia et al.[50] in 2012. The algorithm uses intrinsic motion contrast to detect red blood cells flowing in retinal and choroidal vessels, including the fine capillary networks, and creates angiographic images without intravenous contrast. Previous studies have reported that quantitative analysis of OCT-A can differentiate glaucomatous eyes from normal eyes in analyzing the entire peripapillary vasculature, from ILM to Bruch's membrane.[42] Our findings of decreased annular and global PCD values in the RNFL peripapillary capillaries of glaucomatous patients compared to age-matched normals are similar to recently published data analyzing the entire peripapillary retina.[42] The present

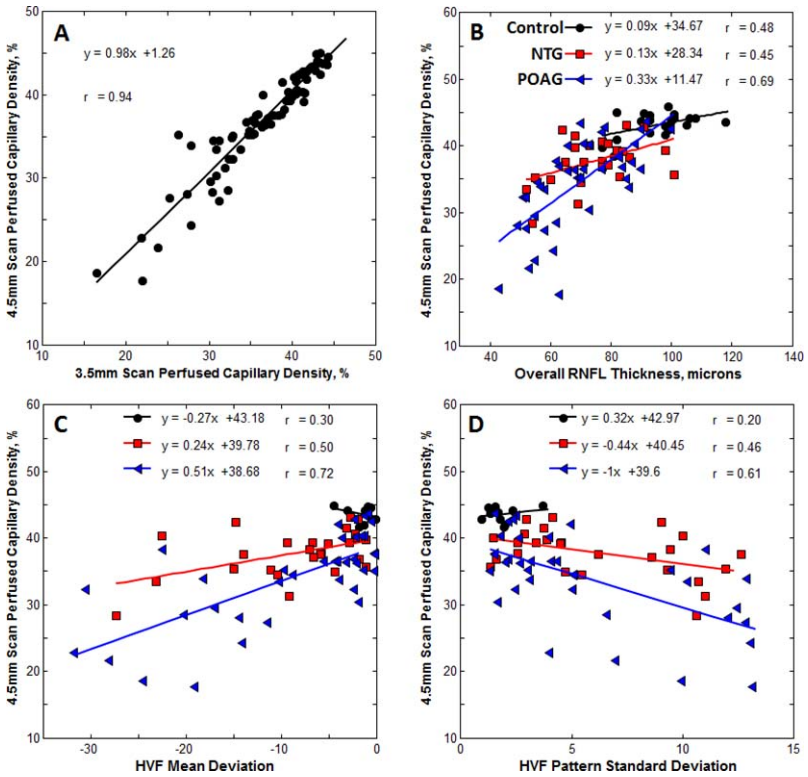

Figure 2. (**A–D**) Graphs display the results of the linear regression analysis used to compare annular PCD in 4.5-mm scans to other clinically relevant information used when assessing glaucoma patients, including overall RNFL thickness, HVF MD, and HVF PSD.

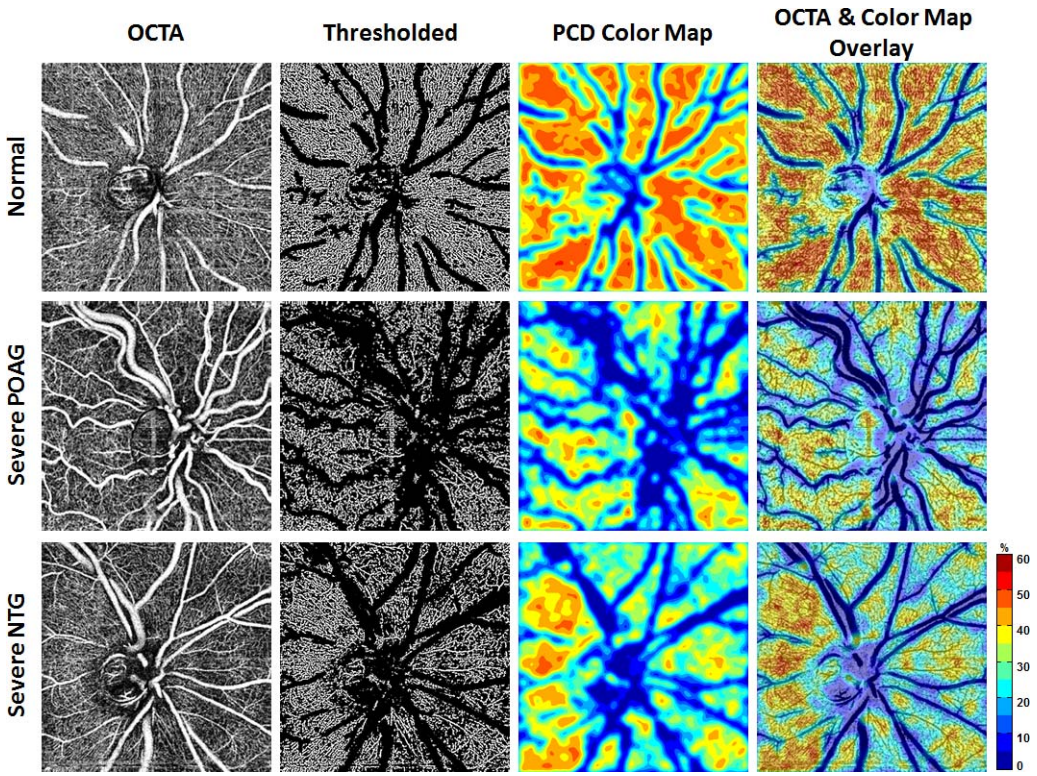

FIGURE 3. Comparisons of 4.5-mm OCT-A images and color-coded perfused capillary density maps in a normal, a severe POAG, and a severe NTG patient. *First column*: grayscale OCT-A images generated using SSADA algorithm. *Second column*: thresholded binary images containing only the perfused capillaries after the removal of major blood vessels. *Third column*: corresponding color-coded perfused capillary density maps. *Last column*: superimposed image of the color maps and the inverted OCT-A images. All images show the temporal peripapillary region on the *left*.

study demonstrates the utility of the Optovue SSADA algorithm and our custom image analysis approach in calculating PCD values and generating color-coded PCD maps of perfused peripapillary capillaries in the evaluation of glaucomatous eyes.

To our knowledge, this is the first study to compare perfused peripapillary capillary densities in POAG and NTG using OCT-A. Both POAG and NTG patients demonstrated decreased PCD values compared to normal patients. While the sample size of our within-group analysis is limited, it appears that PCD declines as glaucoma progresses (Table 6; Figs. 3, 4). We also see a significant difference in PCD values between the POAG and NTG groups, with POAG patients having a lower PCD value than NTG patients. Given the similar distribution of mild, moderate, and advanced glaucoma cases in each group, this difference is less likely to be related to disease stage. It could be related to medication effect, as our POAG group was using a larger number of drops overall, including a larger percentage of patients on medications such as timolol, which may have effects on ocular perfusion pressure.[56,57] This difference could be related to the different pathophysiological processes proposed in normal- and high-tension glaucoma.

Liu et al.[42] suggested that changes in OCT-A peripapillary vessel density may be a reliable diagnostic parameter for detecting glaucoma with similar sensitivities when compared to OCT RNFL thickness. Our findings support their report. This study also introduces the concept of OCT-A color-coded PCD mapping, which offers the advantage of using qualitative data to quickly and easily differentiate normal versus glaucomatous eyes in the clinical setting. Color-coded topographic maps with quantitative data, such as OCT RNFL thickness analysis, have been used successfully by clinicians to evaluate glaucoma patients for many years.[58–60] However, these measurements are limited to detecting evidence of more advanced stages of disease.[33–36,42] We recently described the use of this novel OCT-A mapping technique in perifoveal OCT-A images for quantitative and qualitative grading of diabetic retinopathy.[40] Our current study demonstrates its value for the quantitative and qualitative evaluation of perfused peripapillary capillaries in glaucoma. Optical coherence tomography angiography color-coded PCD maps are as easy to interpret as OCT RNFL thickness maps. We found that the qualitative PCD maps offer a fast method that, along with the quantitative PCD value, can help in the detection of disease. Both POAG and NTG patients have a decrease in perfused vessels compared to normal patients. In comparing the early, moderate, and severe glaucoma patients, regions lacking perfused capillaries expanded as in more advanced stages of glaucoma.

Optical coherence tomography angiography has high within-visit repeatability as well as high between-visit reproducibility. Our findings were previously reported and are consistent with other reports.[40–44,52] One limitation of the device is the difficulty encountered when imaging patients with poor vision or unstable fixation, which may affect repeatability and reliability. Compared to other noninvasive techniques that attempt to measure blood flow using laser Doppler flowmetry or laser speckle flowgraphy, OCT-A appears more reproducible and reliable. Its ease of use translates into a very high interoperator reproducibility compared to other devices.[43,61–67] In this study we chose to use a single operator, but in a clinical practice OCT-A can easily be used by multiple operators with good reproducibility.[42] While OCT-A is not capable of directly measuring blood flow, it offers insights into the perfusion status of the peripapillary region by identifying perfused vessels and quantifying the overall density of perfused vessels. In addition, the color maps

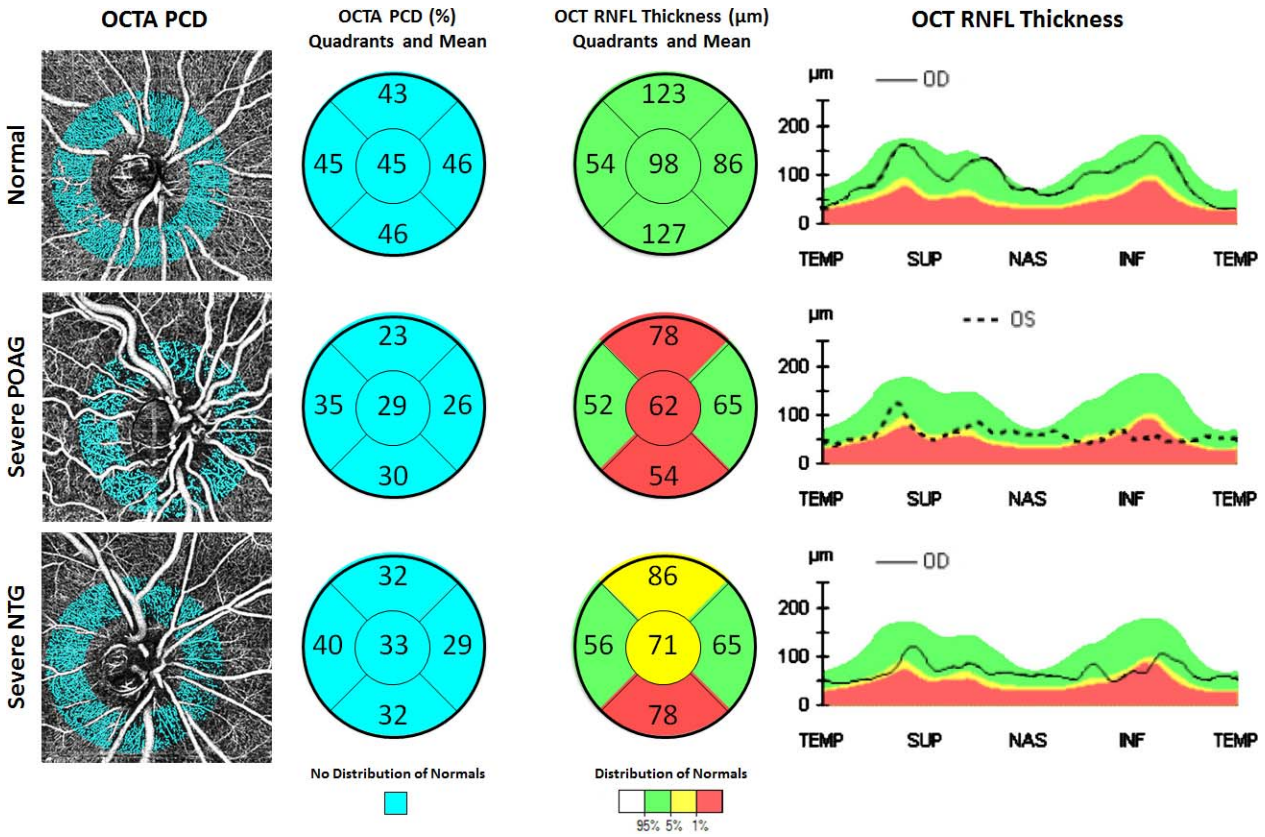

FIGURE 4. Comparisons of peripapillary perfused capillary density and circumpapillary RNFL thickness in the same normal, POAG, and NTG patients shown in Figure 2. *First column*: annular peripapillary capillary area superimposed with 4.5-mm OCT-As. *Second column*: quadrant-specific perfused capillary density of the corresponding OCT-As on the *left*. Mean perfused capillary densities are indicated in the *center. Third column*: quadrant-specific RNFL thickness of the corresponding RNFL thickness plots on the *right*. Mean RNFL thicknesses are indicated in the *center. Last column*: circumpapillary RNFL thickness plots. The OCT-A image of the left eye has been flipped horizontally. All OCT-A images show the temporal peripapillary region on the *left*.

easily identify regions of decreased perfused vessel density. This high-resolution imaging not only is capable of differentiating acquired changes in diseased states, but is also sensitive enough to detect dynamic changes in perfused peripapillary vessels in transient states of hyperoxia.[41]

At the time of our study, OCT-A was capable of capturing both 3.5 × 3.5 and 4.5 × 4.5-mm peripapillary scans. Current software capabilities have expanded to allow 4.5- and 6-mm scans. When comparing the 3.5- and 4.5-mm scans, we found similar PCD values when applying the annular ROI to these images (Table 4). The 3.5- and 4.5-mm annular PCD values correlated very strongly ($r = 0.94$, $P < 0.001$, Fig. 2A). One advantage of using the fixed annular ROI is the ability to improve longitudinal analysis, especially in the setting of slightly decentered images or various scan sizes obtained over time. Interestingly, global PCD analysis of the perfused RNFL peripapillary capillary images after the removal of both the major blood vessels and the inner 1.95-mm circular area (inside the disc) also produced similar results in 3.5- and 4.5-mm scans (Table 5). This suggests that even when image size varies, our custom image analysis approach is capable of producing comparable results. This may allow for improved longitudinal analysis of patients imaged with either 3.5-mm scans, 4.5-mm scans, or a combination of scans acquired over time. Further research is necessary to determine if this translates to the newer 6-mm images as well.

There are a number of limitations to our study. The relatively small sample size and retrospective nature limit the power of our findings. This was also a cross-sectional analysis and patients were not followed over time, so while OCT-A has good repeatability and reliability, we cannot comment on the device's effectiveness in assessing disease progression. In addition, our study was composed mostly of African American and Hispanic patients. While ethnicities were evenly distributed across all groups, it is possible that PCD varies between ethnicities. Other factors that may influence PCD include IOP, medications, and other systemic vascular conditions. Further research is necessary to determine the effects of these variables on PCD values. Another limitation is the acquisition time required for the OCT-A imaging process. In order to obtain images with adequate signal strength, patients must have good fixation and relatively good central acuity. Patients with advanced glaucoma or poor acuity due to other conditions, such as cataracts or macular lesions, are unlikely to have reliable or reproducible results. In addition, further refinements of both the SSADA algorithm and our custom image analysis approach may help improve the concept of perfusion density scaling. Future refinements in the software may serve to assist OCT-A in becoming a standardized imaging modality for the diagnosis and management of glaucoma.

In summary, this study demonstrates that the qualitative and quantitative information provided by OCT-A can differentiate glaucomatous patients from normal patients, and may offer new insights into early diagnosis and a better understanding of glaucoma patients. Optical coherence tomography angiography is an easily interpretable, fast, reliable, noninvasive tool that uniquely permits visualization of perfused peripapillary capillaries, making it an attractive imaging modality for

assessing glaucoma. These findings are the first step in using OCT-A to investigate different patterns of glaucomatous changes in the peripapillary retina, and further research is necessary to determine the role of OCT-A in the detection, monitoring, and characterization of glaucomatous nerve changes according to pathophysiological features.

Acknowledgments

The authors thank the two anonymous reviewers for their helpful suggestions and comments.

Supported in part by an unrestricted grant from Research to Prevent Blindness, Inc., New York, NY, USA. PAS receives support from the David E. Marrus Glaucoma Research Fund and the Herman Peters Pediatric Glaucoma Research Fund of the New York Eye and Ear Infirmary of Mount Sinai.

Disclosure: **N.K. Scripsema**, None; **P.M. Garcia**, None; **R.D. Bavier**, None; **T.Y.P. Chui**, None; **B.D. Krawitz**, None; **S. Mo**, None; **S.A. Agemy**, None; **L. Xu**, None; **Y.B. Lin**, None; **J.F. Panarelli**, None; **P.A. Sidoti**, None; **J.C. Tsai**, None; **R.B. Rosen**, Allergan (C), Clarity (C), Nano Retina (C), Ocata Medical (C), Opticology (F), Optovue (C), Regeneron (C)

References

1. Quigley HA, Broman AT. The number of people with glaucoma worldwide in 2010 and 2020. *Br J Ophthalmol*. 2006;90:262–267.
2. Leske MC. Open-angle glaucoma – an epidemiologic overview. *Ophthalmic Epidemiol*. 2007;14:166–172.
3. Congdon NG, Friedman DS, Lietman T. Important causes of visual impairment in the world today. *JAMA*. 2003;290:2057–2060.
4. Harris A, Rechtman E, Siesky B, et al. The role of optic nerve blood flow in the pathogenesis of glaucoma. *Ophthalmol Clin North Am*. 2005;18:345–353, v.
5. Harris A, Kagemann L, Ehrlich R, et al. Measuring and interpreting ocular blood flow and metabolism in glaucoma. *Can J Ophthalmol*. 2008;43:328–336.
6. Bonomi L, Marchini G, Marraffa M, et al. Vascular risk factors for primary open angle glaucoma: the Egna-Neumarkt Study. *Ophthalmology*. 2000;107:1287–1293.
7. Sung KR, Lee S, Park SB, et al. Twenty-four hour ocular perfusion pressure fluctuation and risk of normal-tension glaucoma progression. *Invest Ophthalmol Vis Sci*. 2009;50:5266–5274.
8. Tobe LA, Harris A, Hussain RM, et al. The role of retrobulbar and retinal circulation on optic nerve head and retinal nerve fibre layer structure in patients with open-angle glaucoma over an 18-month period. *Br J Ophthalmol*. 2015;99:609–612.
9. De Moraes CG, Liebmann JM, Greenfield DS, et al. Risk factors for visual field progression in the low-pressure glaucoma treatment study. *Am J Ophthalmol*. 2012;154:702–711.
10. Leske MC, Connell AM, Wu SY, et al. Risk factors for open-angle glaucoma. The Barbados Eye Study. *Arch Ophthalmol*. 1995;113:918–924.
11. Tielsch JM, Katz J, Sommer A, et al. Hypertension, perfusion pressure, and primary open-angle glaucoma. A population-based assessment. *Arch Ophthalmol*. 1995;113:216–221.
12. Sommer A. Glaucoma risk factors observed in the Baltimore Eye Survey. *Curr Opin Ophthalmol*. 1996;7:93–98.
13. Jonas JB. Association of blood pressure status with the optic disk structure. *Am J Ophthalmol*. 2006;142:144–145.
14. Topouzis F, Coleman AL, Harris A, et al. Association of blood pressure status with the optic disk structure in non-glaucoma subjects: the Thessaloniki eye study. *Am J Ophthalmol*. 2006;142:60–67.
15. Leske MC, Wu SY, Nemesure B, et al. Incident open-angle glaucoma and blood pressure. *Arch Ophthalmol*. 2002;120:954–959.
16. Quigley HA, West SK, Rodriguez J, et al. The prevalence of glaucoma in a population-based study of Hispanic subjects: Proyecto VER. *Arch Ophthalmol*. 2001;119:1819–1826.
17. Leske MC, Warheit-Roberts L, Wu SY. Open-angle glaucoma and ocular hypertension: the Long Island Glaucoma Case-control Study. *Ophthalmic Epidemiol*. 1996;3:85–96.
18. Mitchell P, Lee AJ, Rochtchina E, et al. Open-angle glaucoma and systemic hypertension: the Blue Mountains Eye Study. *J Glaucoma*. 2004;13:319–326.
19. Charlson ME, de Moraes CG, Link A, et al. Nocturnal systemic hypotension increases the risk of glaucoma progression. *Ophthalmology*. 2014;121:2004–2012.
20. Graham SL, Drance SM, Wijsman K, et al. Ambulatory blood pressure monitoring in glaucoma. The nocturnal dip. *Ophthalmology*. 1995;102:61–69.
21. Kaiser HJ, Flammer J, Graf T, et al. Systemic blood pressure in glaucoma patients. *Graefes Arch Clin Exp Ophthalmol*. 1993;231:677–680.
22. Hayreh SS, Zimmerman MB, Podhajsky P, et al. Nocturnal arterial hypotension and its role in optic nerve head and ocular ischemic disorders. *Am J Ophthalmol*. 1994;117:603–624.
23. Hayreh SS, Podhajsky P, Zimmerman MB. Role of nocturnal arterial hypotension in optic nerve head ischemic disorders. *Ophthalmologica*. 1999;213:76–96.
24. Charlson ME, MacKenzie CR, Gold JP, et al. The preoperative and intraoperative hemodynamic predictors of postoperative myocardial infarction or ischemia in patients undergoing noncardiac surgery. *Ann Surg*. 1989;210:637–648.
25. Charlson ME, MacKenzie CR, Gold JP, et al. Intraoperative blood pressure.What patterns identify patients at risk for postoperative complications? *Ann Surg*. 1990;212:567–580.
26. Gold JP, Charlson ME, Williams-Russo P, et al. Improvement of outcomes after coronary artery bypass. A randomized trial comparing intraoperative high versus low mean arterial pressure. *J Thorac Cardiovasc Surg*. 1995;110:1302–1311, discussion 1311–1314.
27. Gillespie BW, Musch DC, Guire KE, et al. The collaborative initial glaucoma treatment study: baseline visual field and test-retest variability. *Invest Ophthalmol Vis Sci*. 2003;44:2613–2620.
28. Tanna AP, Bandi JR, Budenz DL, et al. Interobserver agreement and intraobserver reproducibility of the subjective determination of glaucomatous visual field progression. *Ophthalmology*. 2011;118:60–65.
29. De Moraes CG, Liebmann JM, Park SC, et al. Optic disc progression and rates of visual field change in treated glaucoma. *Acta Ophthalmol*. 2013;91:e86–e91.
30. Chauhan BC, Nicolela MT, Artes PH. Incidence and rates of visual field progression after longitudinally measured optic disc change in glaucoma. *Ophthalmology*. 2009;116:2110–2118.
31. Medeiros FA, Alencar LM, Zangwill LM, et al. Prediction of functional loss in glaucoma from progressive optic disc damage. *Arch Ophthalmol*. 2009;127:1250–1256.
32. De Moraes CG, Prata TS, Liebmann CA, et al. Spatially consistent, localized visual field loss before and after disc hemorrhage. *Invest Ophthalmol Vis Sci*. 2009;50:4727–4733.
33. Abadia B, Ferreras A, Calvo P, et al. Relationship between spectral-domain optical coherence tomography and standard automated perimetry in healthy and glaucoma patients. *Biomed Res Int*. 2014;2014:514948.
34. Wu H, de Boer JF, Chen TC. Diagnostic capability of spectral-domain optical coherence tomography for glaucoma. *Am J Ophthalmol*. 2012;153:815–826.e2.

35. Nilforushan N, Nassiri N, Moghimi S, et al. Structure-function relationships between spectral-domain OCT and standard achromatic perimetry. *Invest Ophthalmol Vis Sci*. 2012;53:2740–2748.
36. Mok KH, Lee VW, So KF. Retinal nerve fiber layer measurement by optical coherence tomography in glaucoma suspects with short-wavelength perimetry abnormalities. *J Glaucoma*. 2003;12:45–49.
37. El Beltagi TA, Bowd C, Boden C, et al. Retinal nerve fiber layer thickness measured with optical coherence tomography is related to visual function in glaucomatous eyes. *Ophthalmology*. 2003;110:2185–2191.
38. Williams ZY, Schuman JS, Gamell L, et al. Optical coherence tomography measurement of nerve fiber layer thickness and the likelihood of a visual field defect. *Am J Ophthalmol*. 2002;134:538–546.
39. Jia Y, Morrison JC, Tokayer J, et al. Quantitative OCT angiography of optic nerve head blood flow. *Biomed Opt Express*. 2012;3:3127–3137.
40. Agemy S, Scripsema N, Shah C, et al. Retinal vascular perfusion density mapping using optical coherence tomography angiography in normals and diabetic retinopathy patients. *Retina*. 2015;35:2353–2363.
41. Pechauer AD, Jia Y, Liu L, et al. Optical coherence tomography angiography of peripapillary retinal blood flow response to hyperoxia. *Invest Ophthalmol Vis Sci*. 2015;56:3287–3291.
42. Liu L, Jia Y, Takusagawa HL, et al. Optical coherence tomography angiography of the peripapillary retina in glaucoma. *JAMA Ophthalmol*. 2015;133:1045–1052.
43. Jia Y, Wei E, Wang X, et al. Optical coherence tomography angiography of optic disc perfusion in glaucoma. *Ophthalmology*. 2014;121:1322–1332.
44. Wang X, Jia Y, Spain R, et al. Optical coherence tomography angiography of optic nerve head and parafovea in multiple sclerosis. *Br J Ophthalmol*. 2014;98:1368–1373.
45. Wang X, Jiang C, Ko T, et al. Correlation between optic disc perfusion and glaucomatous severity in patients with open-angle glaucoma: an optical coherence tomography angiography study. *Graefes Arch Clin Exp Ophthalmol*. 2015;253:1557–1564.
46. Hodapp EA, Parrish RK II, Anderson DR. Clinical decisions in glaucoma. St. Louis: The CV Mosby Co; 1993:52–61.
47. Jia Y, Bailey ST, Hwang TS, et al. Quantitative optical coherence tomography angiography of vascular abnormalities in the living human eye. *Proc Natl Acad Sci U S A*. 2015;112:E2395–E2402.
48. Jia Y, Bailey ST, Wilson DJ, et al. Quantitative optical coherence tomography angiography of choroidal neovascularization in age-related macular degeneration. *Ophthalmology*. 2014;121:1435–1444.
49. Spaide RF, Klancnik JM Jr, Cooney MJ. Retinal vascular layers imaged by fluorescein angiography and optical coherence tomography angiography. *JAMA Ophthalmol*. 2015;133:45–50.
50. Jia Y, Tan O, Tokayer J, et al. Split-spectrum amplitude-decorrelation angiography with optical coherence tomography. *Opt Express*. 2012;20:4710–4725.
51. Kraus MF, Potsaid B, Mayer MA, et al. Motion correction in optical coherence tomography volumes on a per A-scan basis using orthogonal scan patterns. *Biomed Opt Express*. 2012;3:1182–1199.
52. Yu J, Jiang C, Wang X, et al. Macular perfusion in healthy Chinese: an optical coherence tomography angiogram study. *Invest Ophthalmol Vis Sci*. 2015;56:3212–3217.
53. Han IC, Tadarati M, Scott AW. Macular vascular abnormalities identified by optical coherence tomographic angiography in patients with sickle cell disease. *JAMA Ophthalmol*. 2015;133:1337–1340.
54. Bagheri N, Shahlaee A, Sridhar J, et al. En face optical coherence tomography and angiography of talc retinopathy. *Acta Ophthalmol*. 2016;94:103–104.
55. Ishibazawa A, Nagaoka T, Takahashi A, et al. Optical coherence tomography angiography in diabetic retinopathy: a prospective pilot study. *Am J Ophthalmol*. 2015;160:35–44.e1.
56. Oddone F, Rossetti L, Tanga L, et al. Effects of topical bimatoprost 0.01% and timolol 0.5% on circadian IOP, blood pressure and perfusion pressure in patients with glaucoma or ocular hypertension: a randomized, double masked, placebo-controlled clinical trial. *PLoS One*. 2015;10:e0140601.
57. Lee PW, Doyle A, Stewart JA, et al. Meta-analysis of timolol on diurnal and nighttime intraocular pressure and blood pressure. *Eur J Ophthalmol*. 2010;20:1035–1041.
58. Lin SC, Singh K, Jampel HD, et al. Optic nerve head and retinal nerve fiber layer analysis: a report by the American Academy of Ophthalmology. *Ophthalmology*. 2007;114:1937–1949.
59. Mwanza JC, Oakley JD, Budenz DL, et al. Ability of cirrus HD-OCT optic nerve head parameters to discriminate normal from glaucomatous eyes. *Ophthalmology*. 2011;118:241–248.e1.
60. Leung CK, Yu M, Weinreb RN, et al. Retinal nerve fiber layer imaging with spectral-domain optical coherence tomography: patterns of retinal nerve fiber layer progression. *Ophthalmology*. 2012;119:1858–1866.
61. Luksch A, Lasta M, Polak K, et al. Twelve-hour reproducibility of retinal and optic nerve blood flow parameters in healthy individuals. *Acta Ophthalmol*. 2009;87:875–880.
62. Yaoeda K, Shirakashi M, Funaki S, et al. Measurement of microcirculation in the optic nerve head by laser speckle flowgraphy and scanning laser Doppler flowmetry. *Am J Ophthalmol*. 2000;129:734–739.
63. Aizawa N, Yokoyama Y, Chiba N, et al. Reproducibility of retinal circulation measurements obtained using laser speckle flowgraphy-NAVI in patients with glaucoma. *Clin Ophthalmol*. 2011;51171–51176.
64. Shiga Y, Asano T, Kunikata H, et al. Relative flow volume, a novel blood flow index in the human retina derived from laser speckle flowgraphy. *Invest Ophthalmol Vis Sci*. 2014;55:3899–3904.
65. Iester M, Altieri M, Michelson G, et al. Intraobserver reproducibility of a two-dimensional mapping of the optic nerve head perfusion. *J Glaucoma*. 2002;11:488–492.
66. Jonescu-Cuypers CP, Harris A, Wilson R, et al. Reproducibility of the Heidelberg retinal flowmeter in determining low perfusion areas in peripapillary retina. *Br J Ophthalmol*. 2004;88:1266–1269.
67. Kagemann L, Harris A, Chung HS, et al. Heidelberg retinal flowmetry: factors affecting blood flow measurement. *Br J Ophthalmol*. 1998;82:131–136.

Investigative Ophthalmology & Visual Science